

Testing the relativistic Doppler boost hypothesis for supermassive black hole binary candidates

Maria Charisi^{1,2*}, Zoltán Haiman², David Schiminovich², Daniel J. D’Orazio³

¹*TAPIR, California Institute of Technology, Pasadena, CA 91125, USA*

²*Department of Astronomy, Columbia University, New York, NY 10027, USA*

³*Astronomy Department, Harvard University, Cambridge, MA 02138, USA*

15 February 2022

ABSTRACT

Supermassive black hole binaries (SMBHBs) should be common in galactic nuclei as a result of frequent galaxy mergers. Recently, a large sample of sub-parsec SMBHB candidates was identified as bright periodically variable quasars in optical surveys. If the observed periodicity corresponds to the redshifted binary orbital period, the inferred orbital velocities are relativistic ($v/c \approx 0.1$). The optical and UV luminosities are expected to arise from gas bound to the individual BHs, and would be modulated by the relativistic Doppler effect. The optical and UV light curves should vary in tandem with relative amplitudes which depend on the respective spectral slopes. We constructed a control sample of 42 quasars with aperiodic variability, to test whether this Doppler colour signature can be distinguished from intrinsic chromatic variability. We found that the Doppler signature can arise by chance in $\sim 20\%$ ($\sim 37\%$) of quasars in the nUV (fUV) band. These probabilities reflect the limited quality of the control sample and represent upper limits on how frequently quasars mimic the Doppler brightness+colour variations. We performed separate tests on the periodic quasar candidates, and found that for the majority, the Doppler boost hypothesis requires an unusually steep UV spectrum or an unexpectedly large BH mass and orbital velocity. We conclude that at most $\sim 1/3$ rd of these periodic candidates can harbor Doppler-modulated SMBHBs.

Key words: quasars, supermassive black hole binaries,

1 INTRODUCTION

It is well established that most, if not all massive galaxies harbor supermassive black holes (SMBHs) in their nuclei. The mass of the central BH is correlated with several properties of the host galaxy (e.g., velocity dispersion, bulge luminosity, etc.), which suggests that the SMBH and the host galaxy may co-evolve (Kormendy & Ho 2013). In the hierarchical structure formation model, galaxies and quasars are built-up from smaller progenitors through frequent mergers (Haehnelt & Kauffmann 2002). These mergers should result in a supermassive black hole binary (SMBHB) at the center of the newly formed galaxy, surrounded by significant amounts of gas (Barnes & Hernquist 1992).

In the post-merger galaxy, the orbit of the binary shrinks initially due to dynamical friction and subsequently by scattering nearby stars (Begelman, Blandford & Rees 1980). At small (sub-pc) separations, three-body interactions become less efficient, and the binaries may stall for a significant fraction of the Hubble time (see, e.g. Colpi 2014).

In this regime, the ambient gas, which is expected to settle into a circumbinary disc (Barnes 2002), may dominate the binary’s orbital decay (Tang, MacFadyen & Haiman 2017), while, at the same time, it can accrete onto the BHs providing bright electromagnetic emission (e.g. Haiman, Kocsis & Menou 2009). The SMBHB is eventually driven to merger by the emission of low-frequency gravitational waves (GWs), which could be detectable in the future by pulsar timing arrays (PTAs; Manchester & IPTA 2013) and by the space-based interferometer LISA (Amaro-Seoane et al. 2017).

The orbital decay of the binary due to its interaction with the circumbinary disc is expected to be slow (Haiman, Kocsis & Menou 2009; Kocsis, Haiman & Loeb 2012a,b; Rafikov 2013, 2016; Kelley, Blecha & Hernquist 2017) and SMBHBs should spend significant time ($\gtrsim 10^6$ years) at sub-pc separations and thus should be fairly common. Despite their expected abundance, SMBHBs have only been detected at large separations, from several kpc (Komossa et al. 2003; Bianchi et al. 2008; Green et al. 2010; Koss et al. 2011; Fabbiano et al. 2011; Comerford et al. 2011; Fu et al. 2015) down to a few pc (Rodríguez et al. 2006). At sub-pc separations, it is much more difficult to spatially re-

* mcharisi@caltech.edu

solve the orbit of the binary (see, however, D’Orazio & Loeb 2017) and one has to rely on the effects of the binary on its environment. Several candidates have been identified from large velocity offsets in quasar spectra, helical morphology of radio jets, etc (see, e.g., recent reviews by Dotti, Sesana & Decarli 2012 and Komossa & Zensus 2016).

SMBHBs can also be naturally identified as quasars with periodic variability. First, in hierarchical structure formation models, quasars are thought to be activated by galaxy mergers (Kauffmann & Haehnelt 2000). Recent observations of interacting galaxies have provided further evidence for excess AGN activity (Goulding et al. 2017). Many quasars may thus host SMBHBs. Second, numerous hydrodynamical simulations of SMBHBs with circumbinary gas discs have found that such binaries would produce bright quasar-like luminosities, but with the accretion rate modulated periodically at the orbital period of the binary (Artymowicz & Lubow 1996; Hayasaki, Mineshige & Sudou 2007; MacFadyen & Milosavljević 2008; Noble et al. 2012; Roedig et al. 2012; D’Orazio, Haiman & MacFadyen 2013; Farris et al. 2014; Gold et al. 2014). In a binary system, periodic variability can also arise from a precessing jet, as the viewing angle of the jet varies periodically (see, e.g. Kun et al. 2014, 2015).

Recently, a large number of quasars with significant periodicity has emerged, mainly from systematic searches in the photometric databases of large time-domain optical surveys. Graham et al. (2015a, hereafter G15) identified 111 candidates in a sample of $\sim 245,000$ quasars from the Catalina Real-Time Transient Survey (CRTS). Charisi et al. (2016, hereafter C16) analyzed a sample of $\sim 35,000$ quasars from the Palomar Transient Factory (PTF) and identified 33 additional candidates, with typically shorter periods and dimmer magnitudes. Another recent candidate, quasar SDSS J0159+0105, was identified to have two periodic components in its variability with a frequency ratio 1:2 from a smaller sample of ~ 350 low-redshift quasars in CRTS (Zheng et al. 2016).¹

Identifying periodic variability in quasars is extremely challenging, because quasars show stochastic variability. The overall stochastic variability is successfully described by a damped random walk (DRW) model (Kelly, Bechtold & Siemiginowska 2009; Kozłowski et al. 2010; MacLeod et al. 2010) although some recent studies have suggested that a more advanced description of quasar variability may be required (Mushotzky et al. 2011; Zu et al. 2013; Graham et al. 2014; Simm et al. 2016).² Additionally, the optical light curves are typically sparse, with seasonal gaps and relatively short baselines compared to the periods (the identified candidates were typically observed only for a limited number of 2-3 cycles). As pointed out by Vaughan et al. (2016), our incomplete knowledge of quasar variability, in combination

with the limited quality of the optical light curves can lead to false detections of periodicity. This was demonstrated in the case of the quasar PSO J3334.2028+01.4075 (Liu et al. 2015), whose follow-up monitoring failed to show persistent periodicity (Liu et al. 2016). In addition, Sesana et al. (2017) calculated the GW background for the population of SMBHBs implied by the identified periodic binary candidates, and found that it is in tension with the current upper limit derived from PTAs. The tension can be alleviated only if the typical masses and/or the mass-ratios in this sample are surprisingly lower than expected; this suggests that many of the candidates cannot be genuine SMBHBs.

It is therefore crucial to explore additional signatures that could support the binary hypothesis for any periodic candidate. Several such studies followed the discovery of the first quasar with periodic variability (PG 1302-102; Graham et al. 2015b), including the search for multiple periodic components in the optical variability, as expected from hydrodynamical simulations (Charisi et al. 2015; D’Orazio et al. 2015a), the analysis of the helical structure in the radio jet of PG 1302-102 (Kun et al. 2015; Mohan et al. 2016), and the detection of periodic variability in the infrared (Jun et al. 2015; D’Orazio & Haiman 2017).

Another proposed signature of SMBHBs is to detect evidence for the relativistic Doppler boost. Assuming that the observed periodicity corresponds to the redshifted orbital period of the binary, we can infer that most of the candidates are at sub-pc separations, orbiting with mildly relativistic velocities (a few percent of the speed of light). If the optical emission arises in gas bound to the individual BHs, e.g., in mini-discs seen in hydrodynamical simulations (Farris et al. 2014; Ryan & MacFadyen 2017), the luminosity of the brighter mini-disc, typically the circum-secondary disc, will be inevitably Doppler boosted. For near-equal-mass binaries, this Doppler-induced variability is expected to be sub-dominant to hydrodynamically-introduced fluctuations (Bowen et al. 2017a,b; Tang, Haiman & MacFadyen 2018), but for unequal-mass binaries, it could dominate the variability (D’Orazio et al. 2015b).

The observed frequency of the emitted photons will change due to the relativistic motion, whereas the number of photons, which is proportional to F_ν/ν^3 , with F_ν the flux at a specific frequency ν , is Lorentz invariant. The photons will be Doppler boosted by a factor

$$\mathcal{D} = \frac{1}{\gamma \left[1 - \frac{v_\parallel}{c}\right]}; \quad \gamma \equiv \frac{1}{\sqrt{1 - \left(\frac{v}{c}\right)^2}}, \quad (1)$$

where v is the orbital velocity and v_\parallel is its line-of-sight component. Assuming that the emitted radiation has a power-law spectrum $F_\nu \propto \nu^{\alpha_\nu}$, the observed flux will be

$$F_\nu^{\text{obs}} = \mathcal{D}^{3-\alpha_\nu} F_\nu^{\text{em}}. \quad (2)$$

For a binary on a circular orbit, it can be shown that the variability due to Doppler boost to first order in v/c is

$$\frac{\Delta F_\nu}{F_\nu} = (3 - \alpha_\nu) \frac{v}{c} \cos \phi \sin i, \quad (3)$$

where v is the orbital velocity of the more luminous BH (typically the less massive secondary BH, with the primary assumed to contribute negligible flux), i is the inclination of the orbit to the line-of-sight and $0 \leq \phi \leq 2\pi$ is the phase of the orbit.

¹ This quasar was also included in the sample analyzed in G15, but was not identified as periodic. The shortest periodic component of ~ 740 d was identified with both the wavelet and the autocorrelation function analysis in G15, but did not have enough power to be classified as periodic, potentially due to the second periodic component (M. Graham; private communication).

² The periodicity search algorithms and statistical analyses in these papers differ significantly. However, in all cases, the underlying assumption for the quasar variability is the DRW model.

Therefore, even if the optical luminosity in the mini-discs is constant, the unresolved binary will appear blue-shifted (and brighter, for typical spectral slopes, i.e. $\alpha_\nu < 3$), when the more luminous BH is moving towards the observer, and vice-versa. The relativistic Doppler boost may naturally explain the observed light curves, which show smooth quasi-sinusoidal periodicity. We note that the periodic mass accretion rates found in hydrodynamical simulations listed in the Introduction are more bursty than sinusoidal, and are expected to produce more bursty light curves.

The relativistic Doppler boost provides a uniquely robust prediction, which can be tested with multi-wavelength data. For instance, if the UV emission also arises in the mini-discs, then the UV variability should also follow eq. (3). This means that the UV light curve should track the optical, but with a different variability amplitude, which depends on the spectral indices in the respective bands. If the spectrum follows power-laws in both bands with spectral indices α_{opt} and α_{UV} , the relative amplitude follows from eq. (3),

$$\frac{A_{\text{UV}}}{A_{\text{opt}}} = \frac{3 - \alpha_{\text{UV}}}{3 - \alpha_{\text{opt}}}, \quad (4)$$

where, A_{opt} and A_{UV} are the amplitudes of the optical and UV variability.³

D’Orazio, Haiman & Schiminovich (2015) proposed this model to explain the variability of the periodic candidate PG 1302-102. In particular, they found that if PG 1302-102 hosts an unequal mass binary ($q \lesssim 0.05$), orbiting not too far from edge-on ($\lesssim 30^\circ$), the Doppler boost should dominate the variability. The model can successfully fit the observed optical light curve. Additionally, with archival data from the Galaxy Evolution Explorer (GALEX) and the Hubble Space Telescope (HST), they showed that the variability amplitudes in the near-UV (nUV) and far-UV (fUV) bands are $A_{\text{nUV}}/A_{\text{opt}} \sim 2.13$ and $A_{\text{fUV}}/A_{\text{opt}} \sim 2.63$, respectively, consistent with the prediction from eq. (4).

On the other hand, quasars are known to be variable across the electromagnetic spectrum. The optical and UV luminosities typically change almost simultaneously, with minimal interband time-lags (Cutri et al. 1985; Edelson et al. 1996; Giveon et al. 1999; Sakata et al. 2011). Additionally, several studies have indicated that quasars become “bluer-when-brighter” (i.e. the continuum spectral slope becomes steeper in brighter phases); this implies that the variability is wavelength-dependent, with higher variability amplitudes at shorter wavelengths (Kinney et al. 1991; Paltani & Courvoisier 1994; Vanden Berk et al. 2004; Wilhite et al. 2005; Ruan et al. 2014; Hung et al. 2016). For instance, the variability amplitudes in the UV are significantly larger than at optical wavelengths (Welsh, Wheatley & Neil 2011; Zhu et al. 2016).

The above trends suggest that, in general, quasars can show optical/UV variability that may mimic the multi-wavelength variability predicted by the Doppler model (eq. 4). In this paper, we construct a control sample of aperiodic quasars, and determine how often the intrinsic multi-wavelength variability of quasars in this sample produces by

random chance amplitudes consistent with the predictions of the Doppler boost model. Such a test is especially important given that the currently available UV data are typically relatively sparse. More specifically, we analyze optical and UV light curves to determine the ratio of the observed variability amplitudes in the two bands (i.e. the left side of eq. 4). Next, we fit the available optical and UV spectra with power-laws, and from the inferred spectral indices, we compute the expected UV-to-optical amplitude ratio (i.e. the right side of eq. 4). We check whether the above two quantities are consistent within their errors. Additionally, as a separate test, for a subsample of periodic quasars we estimate the UV spectral index required in order for the putative binaries to be Doppler boosted, and compare this to the range of observed UV spectral slopes in the control sample.

This paper is organized as follows: In § 2, we present the construction of the control sample, as well as the sample of periodic candidates, and describe our data analysis. In § 3 we show the results of our analysis, followed by a discussion in § 4. We end with a short summary of our findings and the implications of our results in § 5.

2 SAMPLE AND METHODS

2.1 Sample

In order to statistically assess the significance of an apparent Doppler signature,⁴ our null hypothesis is that this signature can arise from intrinsic wavelength-dependent variability of quasars, unrelated to binary black holes. In other words, we test how often the relative amplitudes of optical and UV variability are by chance consistent with the prediction from eq. (4). For this purpose, we assembled a control sample of quasars and active galactic nuclei (AGNs) that do not exhibit periodic variability, but whose properties (luminosities and redshifts) resemble those of the periodic candidates. In order to perform this Doppler null test, the following data are necessary for each source in the control sample: (1) an optical light curve, (2) a UV light curve, temporally coincident with the optical,⁵ (3) an optical spectrum, and (4) a UV spectrum. Since the availability of UV spectroscopy is limited, we maximized the sample size, starting from a sample of sources with available UV spectra.⁶

More specifically, we made use of two HST spectroscopic catalogs, which provide calibrated co-added UV spectra: (A) the Atlas of Recalibrated HST Faint Object Spectrograph (FOS) Spectra of AGN and Quasars (Evans & Koratkar 2004) and (B) the Cosmic Origin Spectrograph (COS)

⁴ For this test, the Doppler signature refers to the multi-wavelength variability amplitudes described in eq. (4). However, we emphasize that the Doppler model does not refer only to the relative amplitudes, but it can explain the overall variability, e.g., for a circular binary orbit, it can explain the sinusoidal light curve.

⁵ We only considered UV light curves consisting of at least two distinct epochs, separated by 100 days within the optical baseline (see below).

⁶ Light curves in optical and UV bands, as well as optical spectra are available for very large samples of quasars from CRTS, GALEX and SDSS, respectively.

³ The X-ray luminosity also arises very close to SMBHBs and in the binary scenario, it may be Doppler boosted. In this paper, we will focus only on the optical/UV variability, because the available X-ray data are insufficient to extend our study to this band.

quasar catalog of fUV spectra, provided by the Hubble Spectroscopic Legacy Archive (HSLA; [Peeples et al. 2016](#)).⁷ The FOS and COS catalogs include spectra from 204 and 564 unique sources, respectively, among which 56 are common in the two catalogs.

From the COS catalog, we eliminated five sources that we could not cross-correlate in the astronomical database Simbad⁸ and two additional sources that were classified as X-ray binaries. We also excluded from both catalogs sources classified as BL Lac Objects, since they are known to have distinct variability properties from quasars; e.g. their variability may not arise in the accretion disc, but in a relativistic jet ([Edelson 1992](#)). These sources were also excluded from the searches for periodicity in both G15 and C16. We excluded five additional sources from the COS catalog, and one source (PG 1302-102) which was included in both catalogs, because they were identified as periodic.

For the remaining sources, we extracted optical spectra from the Sloan Digital Sky Survey (SDSS),⁹ optical light curves from CRTS¹⁰ and UV light curves from GALEX.¹¹ Since, as mentioned above, light curves and spectra in both bands are necessary for the Doppler test we kept in the sample only the sources that had all the necessary information. We note that GALEX obtained simultaneously photometric measurements with two UV filters (covering the nUV and fUV bands), but the fUV light curves are typically more sparse, because quasars are fainter in fUV. Moreover, the UV spectra usually do not extend to both bands. So if, for instance, the UV spectrum covers only the fUV band, we checked only for the availability of the fUV light curve (with the additional requirement mentioned before, i.e. two distinct epochs and temporal coincidence with the optical data). We note that this step dramatically decreases the sample size; from 528 and 189 sources, in the COS and FOS catalogs (after removing periodic sources and blazars), only 97 and 44 are left after this cut. The main limitation is the availability of UV light curves and even more so the coincidence of those light curves with the optical baseline.

In order to obtain reliable estimates of the spectral slopes, we imposed a redshift cut at $z \leq 0.5$ for the sources examined in the fUV band (sources both from the FOS and COS catalogs) and at $z \leq 1.3$ for the nUV sample (consisting only of sources from the FOS catalog). The redshift cut ensures that the UV continuum is not significantly affected by intergalactic absorption ([Madau et al. 1996](#)). In the fits, we did not consider wavelengths shorter than the Lyman limit. We also excluded nine sources with spectra of very poor quality or with very strong absorption features, since it is difficult to reliably estimate the spectral slopes from those.

Since we estimated the spectral slopes based only on the line-free regions of the spectra (see below), we further

required that the wavelength range of those regions covers at least 25% of the respective GALEX band. As for the GALEX bands, we considered the wavelength range at FWHM of the filter transmission curve extended by 10% at both sides. This choice is dictated by our expectations for the periodic sample; the observed variability amplitude is typically $\sim 10\%$ and is consistent with the putative Doppler boost for the inferred parameters of the binaries.

Given all the above necessary constraints, the test of the null hypothesis was feasible for 42 sources (13 from the COS catalog, 30 from FOS, with one included in both catalogs). The test was feasible in the fUV band for all the sources in the COS catalog and for four of the FOS sources.¹² In the nUV band, the test was performed with the 30 sources from the FOS catalog. In Table 1, we summarize the number of sources included in each band.

2.2 Optical and UV Spectra

We assume that the continuum of quasar/AGN spectra can be approximated by a single power-law $F_\lambda \sim \lambda^{\beta_\lambda}$, where $\beta_\lambda = -\alpha_\nu - 2$. In order to estimate the spectral index, it is essential to avoid the broad emission lines and fit the power-law continuum to the line-free regions of the spectrum, which are known to be significantly less variable than the continuum ([Wilhite et al. 2005](#)). We also emphasize that in the case of SMBHBs, the broad emission lines are likely produced in the circumbinary disc and not in the mini-discs around the individual BHs ([Lu et al. 2016](#)), where the luminosity is expected to be Doppler boosted.

For the optical spectra, we automated the fit taking advantage of the spectral line information provided by the SDSS pipeline. More specifically, each line is fit with a Gaussian profile, and for lines with a valid fit (as indicated by the pipeline), we removed the main part of the line by interpolating between $-\sigma$ to $+\sigma$ from the central wavelength. Subsequently, we smoothed the spectra (to remove potential contribution of the parts of the broad lines that were not removed by the interpolation) by calculating the moving average over a wide window of 400 wavelength bins and fit a power-law to the moving average.

For the UV spectra, on the other hand, the spectral line information is not included in the catalogs. Therefore we identified the line free regions manually, and fit the continuum based on the line-free regions. In both cases, we confirmed the validity of the fit by visual inspection.

If more than one spectrum was available, we used the average slope from all of the spectra. The variability in the spectral slope is demonstrated in the Fig. 4 and 5, with those sources with large horizontal error bars indicating large spectral-slope variability (see also 4.4 below).

2.3 Photometric Fits

We extracted the optical light curves from the public CRTS database (Data Release 2). The survey combines data from three different telescopes and thus the light curves may consist of multiple data streams, which are not calibrated as

⁷ To the best of our knowledge, the above are the only available catalogs with high-level quasar and AGN spectra. Calibrated nUV spectra from COS, and from the Space Telescope Imaging Spectrograph (STIS) will be released in the future in the HSLA (<https://hla.stsci.edu>).

⁸ <http://simbad.u-strasbg.fr/simbad/>

⁹ <https://dr13.sdss.org>

¹⁰ <http://nesssi.cacr.caltech.edu/DataRelease/>

¹¹ <http://galex.stsci.edu>

¹² For these last four sources, the test was feasible both in the fUV and nUV bands.

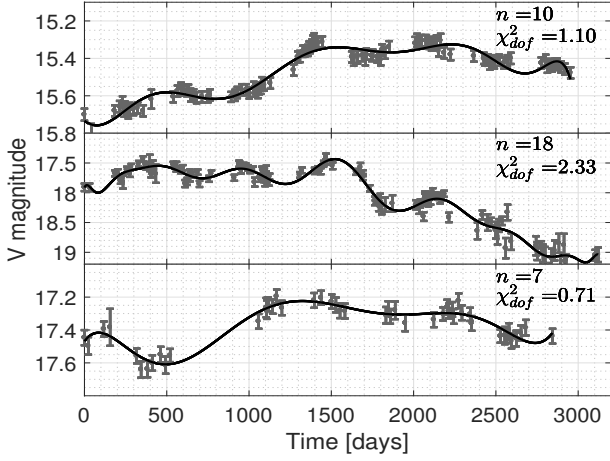


Figure 1. Examples of optical light curves and the chosen polynomial fits with $\chi^2_{\text{dof}} \sim 1$ (top panel), $\chi^2_{\text{dof}} > 1$ (middle panel), and $\chi^2_{\text{dof}} < 1$ (bottom panel). The degree of the polynomial n is also shown in each panel.

a single light curve. In order to avoid systematic effects, we selected the single light curve with the highest number of observations. Additionally, the CRTS light curves contain four data points per night (four observations per visit separated by 10 min). Since the short-term variability is not significant for this study, we binned the observations taken within the same night. Next, we extracted UV light curves from GALEX. These light curves, especially in the fUV band, are typically sparse with only a handful of epochs.

The next step consisted of measuring the relative amplitudes in the optical and UV bands (left side of eq. 4). This step is challenging for two main reasons: (1) quasars exhibit stochastic variability, and (2) the optical and UV data were not taken simultaneously. To address these issues, we approximated the optical variability with an n^{th} degree polynomial. We chose the order of the polynomial between 5 and 20 based on the reduced χ^2 (we chose the smallest polynomial order which gives $\chi^2_{\text{dof}} \sim 1$) combined with visual inspection of each fitted light curve, to ensure that the chosen fit reasonably represents the variability. For instance, in some cases, the reduced χ^2 is smaller than unity ($\chi^2_{\text{dof}} < 1$) for all the tested polynomials, which may suggest that the provided error bars are overestimated, whereas, in other cases, it is always higher than unity ($\chi^2_{\text{dof}} > 1$), because the polynomial fit cannot entirely capture the short-term variability. In Fig. 1, we show three optical light curves with the chosen polynomial fit, with $\chi^2_{\text{dof}} \sim 1$ (top panel), $\chi^2_{\text{dof}} > 1$ (middle panel), and $\chi^2_{\text{dof}} < 1$ (bottom panel). The order of the chosen polynomial is also shown in each panel.

We fit the UV light curve by rescaling the optical fit and shifting it by a constant,

$$y_{\text{uv}}^n = \theta_1 \times y_{\text{opt}}^n + \theta_2. \quad (5)$$

Note that $y_{\text{uv}}^i \equiv y_{\text{uv}}(t^i)$, where t^1, t^2, \dots, t^n represent the time series of the UV measurements, and $y_{\text{opt}}(t^n)$ are the optical light-curves interpolated to these times using the polynomial fits. This can be re-written in matrix notation as

$$Y_{\text{uv}} = M \times \Theta, \quad (6)$$

where

$$Y_{\text{uv}} = \begin{bmatrix} y_{\text{uv}}(t^1) \\ y_{\text{uv}}(t^2) \\ \vdots \\ y_{\text{uv}}(t^n) \end{bmatrix}, \quad M = \begin{bmatrix} y_{\text{opt}}(t^1) & 1 \\ y_{\text{opt}}(t^2) & 1 \\ \vdots & \vdots \\ y_{\text{opt}}(t^n) & 1 \end{bmatrix}, \quad \Theta = \begin{bmatrix} \theta_1 \\ \theta_2 \end{bmatrix}. \quad (7)$$

The maximum likelihood solution for this regression is

$$\Theta = \left(M^T \times C^{-1} \times M \right)^{-1} \times \left(M^T \times C^{-1} \times Y_{\text{uv}} \right) \quad (8)$$

where C is the covariance matrix of the UV measurement errors.

We emphasize that the polynomial fit provides a reasonable way for interpolating the light curves, but it does not have predictive power outside the observed time interval. Therefore, as mentioned above, UV data points that do not overlap with the optical were excluded from the fit.

2.4 Periodic Sample

We extracted UV light curves and optical spectra for the sample of periodic quasars from G15 and C16. As mentioned above, with the exception of PG 1302-102, which was analyzed in D’Orazio, Haiman & Schiminovich (2015), only five of the periodic sources in G15 have UV spectra. Among those, four do not have multiple UV observations from GALEX and one has multiple observations in nUV, whereas the spectrum covers the fUV band. Therefore, directly testing the Doppler model was not possible for any of the periodic sources. However, for the sub-sample of sources that have UV light curves and optical spectra (55 out of 111 sources in G15 and 13 out of 33 sources in C16), we were still able to assess whether the Doppler boost model is feasible.

More specifically, assuming that the optical and UV variability are both dominated by the effects of relativistic Doppler boost, we inferred the implied UV spectral index from eq. (4). We were able to estimate the nUV spectral index for 68 sources and for 27 of these sources we were also able to calculate the fUV spectral index, see also Table 1. For this, we followed the steps described above for fitting the optical spectra with a power-law (in the V band for CRTS and the R band for PTF) and finding the relative amplitude of UV and optical variability.¹³ Subsequently, we compared our estimates including the 1- σ uncertainties to the distribution of measured slopes from the control sample to assess whether the inferred spectral slopes correspond to realistic values seen in quasars with similar properties.

As we mentioned above, the Doppler signature is not limited only to the multi-wavelength prediction from eq. (4). If the emission of the periodic candidates is indeed due to relativistic Doppler boost, the model should explain the entire sinusoidal variability of the optical light curve as well. For the candidates that have at least one optical spectrum (17 from the PTF sample and 94 from the CRTS sample), we additionally checked whether the Doppler model is feasible

¹³ Since the optical light curves of the periodic sources are described by sinusoids, when fitting the UV light curves, we included UV data points outside of the optical baseline. This was not possible for the stochastic variability of quasars in the control sample.

Table 1. Number of sources with available data in the different bands in the control and periodic sample.

	Optical	nUV	fUV	nUV+fUV
Control Sample	42	30	16	4
Periodic Sample	68	68	27	27

based only on the optical variability. To perform this check, we computed the ratio of the maximum possible Doppler boost amplitude (for the given parameters of the putative binaries) to the observed optical variability amplitude.

In more detail, as is obvious from eqs. (1) and (3), the maximum Doppler boost occurs when the line-of-sight velocity is maximum, which in turn occurs when the binary orbit is edge-on, i.e. $\sin i = \sin(\pi/2)$. Additionally, the orbital velocity of the secondary in a binary system depends on the mass ratio q ,

$$v_2 = \left(\frac{1}{1+q} \right) \left(2\pi \frac{GM}{P} \right)^{1/3}, \quad (9)$$

and the maximum Doppler boost corresponds to this orbital velocity in the limit of a very unequal mass binary (i.e. $q \rightarrow 0$). In this most optimistic case, the Doppler factor is maximum (minimum), when the secondary moving towards (away from) the observer,

$$D_{\max} = \frac{1}{\gamma \left[1 - \left(2\pi \frac{GM}{c^3 P} \right)^{1/3} \right]}, \quad (10)$$

$$D_{\min} = \frac{1}{\gamma \left[1 + \left(2\pi \frac{GM}{c^3 P} \right)^{1/3} \right]}. \quad (11)$$

For each SMBHB candidate, the orbital period P is known (assuming that the observed period is the redshifted orbital period). The total mass M was either measured from the width of the broad emission lines or estimated from the quasar's luminosity as in C16. The optical spectral slope α_{opt} , and the observed variability half-amplitude in magnitudes, A_{opt} , were measured directly from the optical spectra and the light curves, respectively.

Based on the above, the ratio of the maximum possible range under the Doppler hypothesis to the observed variability range is given by

$$\begin{aligned} \frac{A_{\text{Dop}}(M, P, \alpha_{\text{opt}})|_{\max}}{2A_{\text{opt}}} &= \frac{-2.5 \log_{10} [F_{\text{opt}}^{\max}/F_{\text{opt}}^{\min}]}{2A_{\text{opt}}} \\ &= \frac{-2.5 \log_{10} (D_{\max}/D_{\min})^{3-\alpha_{\text{opt}}}}{2A_{\text{opt}}}. \end{aligned} \quad (12)$$

If this ratio is below unity for a given SMBHB candidate, the periodicity associated with that candidate cannot be generated solely by relativistic Doppler boost.

3 RESULTS

3.1 Null Hypothesis Test in Control Sample

We tested the null hypothesis that an apparent Doppler boost signature described by eq. (4) arises by chance, given the chromatic variability of quasars. For this test, we checked whether the relative variability amplitudes measured directly from the light curves (left side of the equation) are

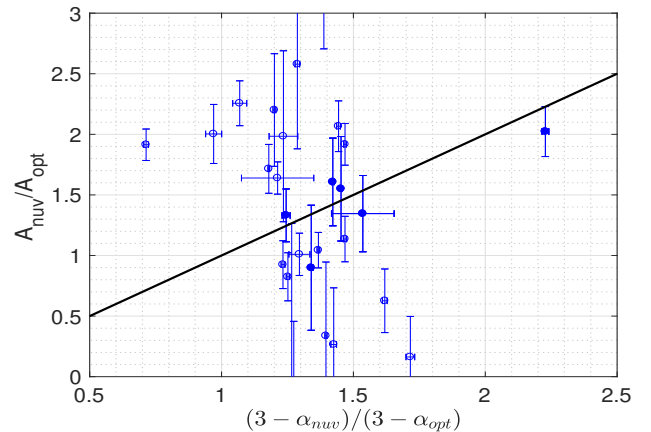


Figure 2. The ratio of variability amplitudes in the nUV and optical bands, measured directly from the light curves *versus* the amplitudes expected from relativistic Doppler boost, calculated from the measured spectral indices in the two bands. The equality line corresponds to the Doppler-boost prediction from eq. (4). The filled symbols indicate sources that are consistent with this Doppler signature within their $1\text{-}\sigma$ error.

equal (within their $1\text{-}\sigma$ uncertainty) to the relative amplitudes predicted from the Doppler effect, which depends on the respective spectral slopes (right side of the equation). In Fig. 2, we show the measured ratio of the nUV to the optical variability amplitude, *versus* the Doppler-boost prediction calculated from the measured spectral slopes, for the 30 quasars for which all necessary data were available. We also show the equality line for comparison, and we indicate the sources for which the variability is consistent with eq. (4) by filled symbols. In total, in the nUV band, we found that the variability is consistent with the Doppler prediction in 6 out of 30 quasars. This means that the Doppler boost signature can be observed by chance in $P(nUV) \equiv 20^{+8\%}_{-6\%}$ ¹⁴ of the quasars in the sample.

We next repeated the above test for quasars in the fUV band. In Fig. 3, we show the amplitude ratio of fUV and optical variability *versus* the value expected from a Doppler boost in this band. Triangles correspond to data from the COS catalog, circles to the data from FOS, and the diamond symbol marks the one AGN which was included in both catalogs (the UV slope for this source was calculated as the average slope from the two spectra). Again, we indicate the sources for which variability is consistent with eq. (4) by filled symbols. In this case, we found that 6 out of 16 are consistent with eq. (4), i.e. an apparent Doppler signature can arise by random chance $P(fUV) \equiv 37.5^{+12.5\%}_{-11.5\%}$ of the time.

We also note that the data are randomly scattered and do not show any significant correlation. More importantly for our purposes, the overall trends in the data, using either the fUV or the nUV bands, do not follow eq. (4), delineated with the equality line. In fact, the Pearson correlation coefficient for the nUV (fUV) sample is -0.23 (-0.69). This is clearly illustrated in Figures 2 and 3, and suggests that

¹⁴ We calculated the $1\text{-}\sigma$ confidence intervals with the Wilson (score) method (Wilson 1927).

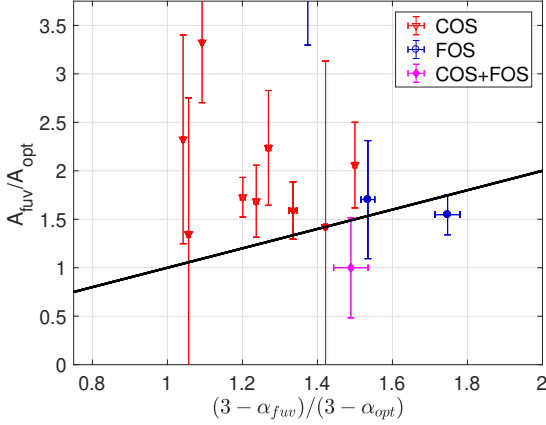


Figure 3. Null hypothesis test for the Doppler boost signature, as in Fig. 2, but in the fUV band. Red triangles correspond to data from the COS catalog, blue circles to data from FOS and the purple diamond to the one AGN with spectra from both FOS and COS. As in Fig. 2, filled symbols illustrate the sources which satisfy eq. (4).

the cases which satisfy the Doppler prediction from eq. (4) should be due to chance coincidence owing to the limited and noisy data. In other words, the relatively high probability of the Doppler-like signature arising by chance simply reflects limitations of the best available control sample, and not necessarily the intrinsic properties of chromatic AGN variability. The clear conclusion is that higher quality temporally coincident optical and UV light curves and spectra, for a larger number of aperiodic AGN, must be collected in the future.

3.2 Doppler Boost in Periodic Sample

For a sub-sample of 68 periodic sources (55 from G15 and 13 from C16), which had available UV light curves and optical spectra, we calculated the UV spectral indices that would be required in order for their variability to be consistent with relativistic Doppler boost. For all the above sources, we calculated the spectral index in the nUV band, while for 27 of those (20 from G15 and 7 from C16), we were also able to calculate the spectral slope in the fUV band. Subsequently, we compared the estimated UV indices, including their $1\text{-}\sigma$ error, with the observed distribution of spectral slopes in the respective band in the control sample.

In Figures 4 and 5, we show the inferred nUV and fUV slopes, respectively. We illustrate with circles the sources for which we could calculate the spectral index only in the nUV band, whereas with triangles we show the sources for which both spectral slopes could be calculated. Filled symbols present sources with spectral indices that are consistent within $1\text{-}\sigma$ with the distribution of spectral slopes observed in the control sample (filled circles: only the nUV index was calculated and is consistent; filled triangles: both indices were calculated and both were consistent with the observed distributions) and open symbols present sources with indices that are inconsistent with the observed distributions. In the case that both slopes were determined, open triangles demonstrate sources that are inconsistent in both

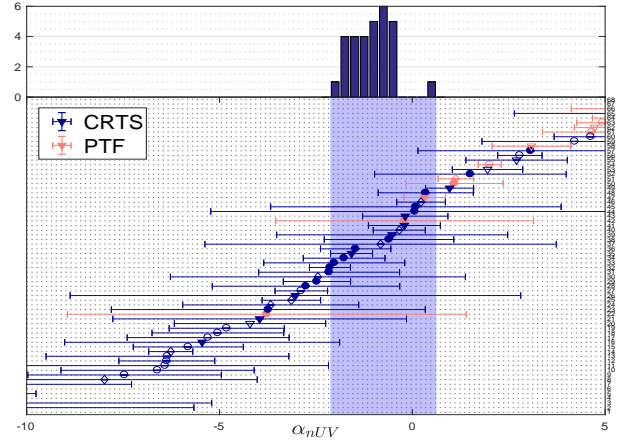


Figure 4. *Top panel:* Distribution of nUV spectral indices measured from HST spectra for the sources in the control sample. *Bottom panel:* Inferred nUV spectral slopes for periodic quasars, assuming Doppler boost variability; filled (open) symbols for spectral indices consistent (inconsistent) with the observed distribution, circles when only the nUV spectral index was calculated, triangles when both nUV and fUV spectral slopes are calculated. We illustrate with open diamonds the sources the spectral indices of which are consistent with the observed slopes in one band but not in the other. Blue symbols present CRTS sources from G15 and red for PTF sources from C16. The indices on the right side of the plot refer to the entries in Table 2. The shaded region delineates the range of the observed distribution shown in the top panel.

bands, whereas open diamonds illustrate the sources that are consistent in one band but not in the other. We color-code the periodic sources from CRTS with blue symbols and the sources from PTF with red. For clarity, we rank-ordered the sources based on their inferred nUV and fUV slope, respectively. The numbers on the right side of the figure refer to the entries in Table 2 below, in which we present the details of the analysis for the periodic sample. On the top panel in both Figures 4 and 5, we show for comparison the distribution of measured UV slopes from the control sample in the respective band. The shaded regions in the bottom panels delineate the full ranges of these distributions.

We found that 31 out of 68 sources (or $46^{+6}_{-6}\%$) are consistent with the observed distribution if we consider only the nUV slopes, and 15 out of 27 (or $55^{+10}_{-9}\%$) when considering only the fUV spectral indices. If we require that both measured spectral indices are consistent with their respective observed distributions, then we find 9 out of 27 sources (or $33^{+10}_{-8}\%$) pass both tests. These fractions are higher than expected based on the random multi-wavelength variability found above. This test, of course, can be used only to *rule out* the Doppler hypothesis for $\sim 2/3$ rd of the sample. Although the remaining $\sim 1/3$ rd of the sample remains consistent with the Doppler boost, it is necessary to obtain their UV spectra, and directly measure their spectral slopes, to check this. Another caveat is that we are comparing to the distribution observed in our small control sample; the entire population of quasars likely has a wider distribution of spectral slopes. Therefore, it is possible that we excluded some sources that could be Doppler boosted. In principle, this slope-distribution could be measured for many more

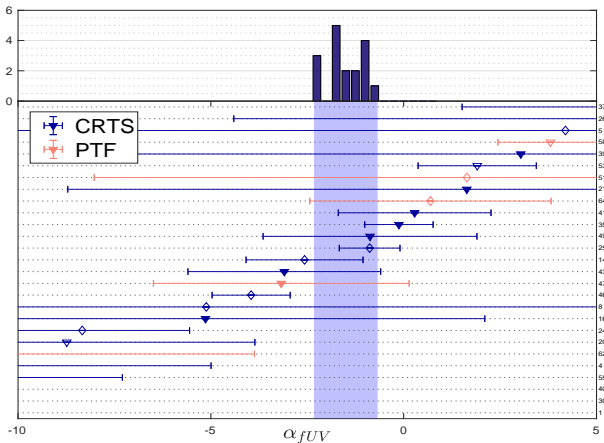


Figure 5. Same as Fig. 4, but in the fUV, instead of the nUV. All the sources in this sample have inferred spectral slopes in both UV bands.

sources beyond the control sample we assembled, i.e. objects with available UV spectra but without a suitable UV light-curve.

Finally, we calculated whether the observed optical variability amplitude is consistent with the maximum value allowed by a relativistic Doppler boost (eq. 12). We found that for 76 out of 94 sources from G15 and 18 out of 25 from C16 the ratio is above unity and thus the Doppler boost model is feasible. We show the estimated ratio in Table 2. We were able to exclude 5 additional sources, which, based on the spectral indices, could be consistent with the Doppler model (filled symbols in the Figures above), because they failed this criterion (i.e. the ratio is below unity). This clearly demonstrates that tests of the Doppler model should not be limited to the relative amplitudes from eq. (4), but should require the model to explain the overall optical and UV variability of the sources to begin with.

4 DISCUSSION

4.1 Expanding the sample size: UV spectral slope from photometric data?

One of the main limitations of the current study is the small size of the sample for which the test was feasible: all of the necessary spectral and photometric information was available only for 42 sources. As mentioned above, this is primarily driven by the lack of UV spectra. On the other hand, for many of the sources without a UV spectrum, photometric data exists in the two UV bands of GALEX. It is therefore natural to ask if we could obtain reliable estimates of the UV spectral slopes for these sources (e.g., by using spectral templates), and thereby increase the sample size significantly.

Under the approximation that the continuum throughout the entire UV band can be described by a single power-law, a single GALEX observation with simultaneous photometric measurements in both the nUV and the fUV bands determines the power-law slope. Such measurements are available for a large number of quasars and AGN. We assessed the validity of this approach, using the sources in

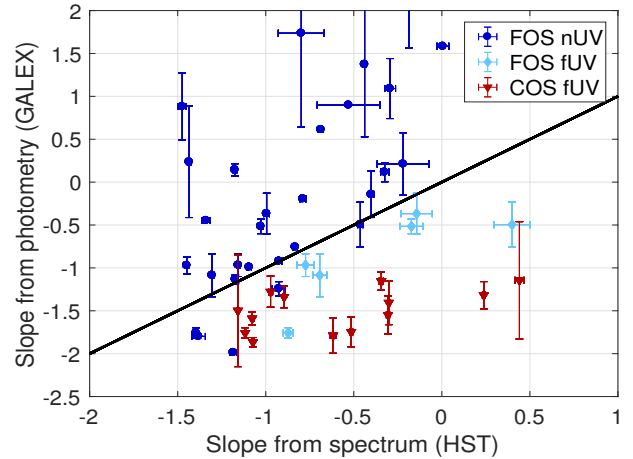


Figure 6. Spectral slopes estimated from GALEX photometric data *versus* measured by fitting HST spectra with a power-law. Dark blue circles: nUV spectra from FOS; light-blue diamonds: fUV spectra from FOS; red triangles: fUV spectra from COS.

the control sample, by calculating spectral indices from the photometry and comparing with the measured slopes.

We first calculated the photometric flux in each band (see https://asd.gsfc.nasa.gov/archive/galex/FAQ/counts_background.html),

$$F_{nUV} = 2.06 \times 10^{-16} \times 10^{\left(-\frac{m_{nUV}-20.08}{2.5}\right)}, \quad (13)$$

$$F_{fUV} = 1.40 \times 10^{-15} \times 10^{\left(-\frac{m_{fUV}-18.82}{2.5}\right)}, \quad (14)$$

and subsequently the spectral slope in the UV band, assuming that the fluxes are measured at the effective wavelengths $\lambda_{fUV}^{\text{eff}} = 1542.26\text{\AA}$ and $\lambda_{nUV}^{\text{eff}} = 2274.37\text{\AA}$, respectively. If the UV light curve had multiple simultaneous observations in both bands, we calculated an average of the spectral slopes measured from each individual epoch.

In Fig. 6, we present these photometric estimates of the spectral indices *versus* the true slopes measured directly from HST spectra. Dark blue circles and light blue diamonds indicate data from the FOS catalog in the nUV and fUV bands, respectively, and red triangles show fUV data from the COS catalog. The equality line is also shown for comparison. We see that the slopes inferred from photometry are not strongly correlated with the slopes measured directly from the spectra. The spectral slopes tend to be overestimated compared to the measured ones in the nUV band and underestimated in fUV. Since the slope calculated from photometry is roughly similar to the average of the spectral slopes in the two bands, this trend is not surprising given that the spectra tend to be steeper in the nUV band and relatively flatter in fUV.¹⁵

While in principle, a more complicated spectral template (in place of a single power-law) could account for this curvature, the large scatter in Fig. 6 clearly precludes accurate photometric estimates. The large scatter may be partly caused by the presence of broad emission lines, which affect the calculation of the photometric fluxes and thus the spectral indices. Depending on the redshift of the source, a

¹⁵ We note that the spectral slopes β_λ are typically negative, as is also obvious from the figure.

different set of lines are present in each of the broad-band filters of GALEX and since our sample covers a wide redshift range, it is complicated to account for this effect.

Another possibility would be to calculate the UV spectral indices from spectral templates (e.g. Shull, Stevans & Danforth 2012; Ivashchenko, Sergijenko & Torbaniuk 2014). However, as shown in Figs. 4 and 5, the observed distribution of measured spectral slopes is relatively broad. Additionally, the variance of the spectral indices observed in quasars with multiple spectra (mainly optical) is significant. Hence, we expect that using a spectral template will not be sufficient for this study, since it will not allow us to capture the spectral variability of each quasar, which is crucial for our test.

For all the above reasons, we concluded that the expansion of the sample using spectral slopes estimated from photometry is not possible. However, we expect that the test will be feasible for a larger sample of quasars in the near-future, once the co-added spectra from STIS and the nUV spectra from COS become available in HSLA. A complementary approach is to acquire UV spectroscopy for a sample of quasars that already have well-sampled UV and optical light curves. In fact, this may be the most time-efficient strategy to improve the null hypothesis test presented here: acquiring well-sampled UV/optical light curves for quasars that have UV and optical spectra would require multi-year campaigns, whereas UV spectra (and potentially optical spectra as well) for the already well-sampled light curves could be obtained without a long wait.

4.2 Null test in both UV bands

In § 3.1, we showed that the probability for the Doppler signature from eq. (4) to occur by random chance is $P(\text{nUV}) = 20^{+8}_{-6}\%$ and $P(\text{fUV}) = 37.5^{+12.5}_{-11.5}\%$ for the samples examined in the nUV and fUV band, respectively. However, there are four sources in the control sample, for which the null hypothesis test was feasible in both bands. Of these, one is consistent with eq. (4) in both bands, one is not consistent in either band and the remaining two are consistent with the Doppler signature only in the fUV band, but not in the nUV band. From this sample, we can conclude that the probability that the Doppler signature from eq. (4) can arise by chance in both bands simultaneously is $P(\text{nUV} \cap \text{fUV}) = 25^{+25}_{-15}\%$. It is also worth noting that the source which is consistent with the Doppler signature in both bands is the only source which has two fUV spectra from FOS and COS and the spectral index is calculated as the average of the two. If we consider only the FOS spectrum (in the other three cases, both the nUV and fUV slopes are calculated from the same co-added spectra from FOS), the source is inconsistent with eq. (4) in the fUV.

As this last point illustrates, in this sub-sample, we are particularly limited by small number statistics and sparse data; this unfortunately precludes drawing conclusions from four sources about the entire quasar population. We note further that stochastic variations in the nUV and fUV spectral slopes are likely to be correlated, and this correlation would need to be quantified and taken into account, when performing a joint null-test in the nUV and fUV bands. This joint test would be valuable, since the Doppler model, in principle, should account for variability in both UV bands.

It would therefore be particularly important to obtain simultaneous nUV and fUV data on a larger set of objects.

4.3 Variability amplitudes

As mentioned above, another major limitation in the present study arises from the very sparse UV light curves. Most of the GALEX light curves have only 2-3 distinct epochs temporally coincident with the optical baseline. This strongly affects the estimates of the relative amplitudes, as is demonstrated by the large error bars in Figs. 2 and 3. This limitation is more severe in the fUV band, where the light curves rarely sample more than two epochs, and the photometric uncertainties are larger. In fact, the larger uncertainties in the relative amplitudes, in combination with the smaller sample size, likely explains why the Doppler signature can be observed by chance more often in the fUV band (i.e. $\sim 20\%$ in nUV *vs.* $\sim 37\%$ in fUV).

Because of the small number of UV observations, our ability to constrain the UV/optical amplitudes can also be limited by “unfortunate” sampling. In order to illustrate this, consider a UV light curve with only two epochs and the following extreme cases: (1) the UV data points correspond to two epochs with very similar optical magnitudes and (2) the UV data points trace the maximum and minimum magnitude of the optical light curve. In the first case, it is almost impossible to constrain the relative UV/optical amplitude, whereas in the latter case, the amplitude is uniquely constrained. This is an additional uncertainty incorporated into the large error bars in Figs. 2 and 3.

Finally, for the available light curves, the optical and UV data were not taken simultaneously. This further limits our ability to estimate the relative variability amplitudes, because quasars show short-term variability (e.g. Kelly, Bechtold & Siemiginowska 2009).¹⁶ This is not included in our analysis, because our polynomial fits effectively filter out the short-term variability of the optical light curves. However, constructing light curves with simultaneous measurements in optical and UV bands, which can be attained with an instrument like the Ultraviolet/Optical Telescope (UVOT) on Swift, can mitigate this issue and significantly improve our UV/optical fits. Note that in the Doppler boost model, this short-term variability can be explained only if the rest-frame luminosities of the mini-discs fluctuate, e.g., due to variable accretion rate.

4.4 Constant Spectral Slope

Throughout our analysis, we assumed that the spectral slopes do not evolve with time. An intrinsically time-variable spectral slope could, in principle, be easily incorporated in the Doppler-boost model. However, in practice, the assumption of a constant intrinsic spectrum is necessary, because of the lack of multiple UV and optical spectra for each source.¹⁷

¹⁶ Short-term variability here refers to timescales of several days to a couple of months and not the variability between 1-10 d which Caplar, Lilly & Trakhtenbrot 2017 found to be overestimated due to the limited photometric precision of the time domain surveys.

¹⁷ In the ideal case, we would test the Doppler signature with simultaneous UV and optical spectra.

Since the ultimate goal is to assess whether we can differentiate the Doppler-boost variability from the intrinsic chromatic variability, it is crucial to understand the importance of this limitation.

To investigate this issue, we consider the sample of quasars that have multiple spectroscopic observations. There are seven sources with more than one spectrum in the optical, and one source with two fUV spectra. In Fig. 2 and 3, these sources can be recognized from their large horizontal error bars (the error in the spectral slope from a single spectrum is typically small, as seen in the figures for the other sources). From these figures, we conclude that the error introduced by a variable spectral slope is significantly smaller compared to the uncertainty in constraining the relative amplitudes.

4.5 Further improvements of the Doppler tests

Since the chromatic variability of quasars does not appear correlated with the Doppler prediction from eq. (4), it is reasonable to assume that with good quality data (a sufficient number of data points, low photometric noise, simultaneous optical and UV spectra) the variability caused by relativistic Doppler boost could be distinguished much more easily from intrinsic variability. In other words, our main result, namely that the Doppler signature can arise by chance as often as in $\sim 20\%$ ($\sim 37\%$) of quasars in the nUV (fUV) bands, likely reflects mainly the limited quality of the currently available data.

A significant improvement could be achieved by increasing the size of the control sample, especially if we can increase the number of sources for which the null hypothesis can be tested simultaneously in both the nUV and the fUV band. In this study, we assembled the control sample starting from the sources that already had measured UV spectra. However, as discussed in § 2.1 the requirement for UV light curves coincident with the optical baseline was yet another major limitation on the size of the control sample. Likewise, a further limitation results from the large error bars in fitting the relative amplitudes of the optical and UV light curves, mainly due to the small number of UV data points. These limitations could be addressed by first assembling a sample of quasars that have well-sampled UV light-curves (in both nUV and fUV) temporally coincident with existing optical light-curves, and then obtain UV spectra for these sources, covering both bands.

Finally, in order to incorporate additional uncertainties arising from the short-time variability of quasars, we could start from quasars that have good quality UV spectra, and then construct well-sampled optical and UV light curves with simultaneous observations. This can be achieved with a telescope such as UVOT on the Swift satellite. However, this would generally require a long wait; i.e. a multi-year campaign to build up reasonably long baselines.

5 SUMMARY

Relativistic Doppler boost is inevitable in compact SMBHBs, and provides a unique multi-wavelength test for the binary nature of any SMBHB candidate. Here we examined this test in the context of binary candidates identified as

quasars with periodic optical variability. Our main conclusions can be summarised as follows.

- We assembled a control sample of 42 quasars with aperiodic variability, and analysed it to test whether the Doppler boost signature is distinct from intrinsic chromatic brightness variability.
- We found that in the best available control sample, variability consistent with the Doppler model can arise by chance for $\sim 20\%$ and $\sim 37\%$ of the quasars in the nUV and fUV band, respectively. The larger chance of coincidence is likely explained by the poorer quality of the fUV data.
- For 68 SMBHB candidates identified as quasars with periodic variability, based on their optical/UV light curves and optical spectra, we calculated the UV spectral slopes that would be required for the periodicity to be caused by relativistic Doppler boost.
- Of these, 26 sources could be explained by relativistic Doppler boost, since their inferred slopes are consistent with the observed range of spectral indices from the control sample.
- We were additionally able to exclude 5 of the above sources, because even the most optimistic Doppler model cannot produce variability amplitudes as large as observed in the optical.

Overall, our paper suggests that quasars do not often mimic the optical/UV colour-variations expected to arise from relativistic Doppler boost. We have also demonstrated the need for a larger and better control sample. With a sufficient number of UV data points, low photometric noise, and simultaneous optical and UV spectra, such an improved control sample could be constructed, and would allow an improved test, conclusively ruling out that a Doppler colour signature arises by chance from stochastic intrinsic variability.

ACKNOWLEDGEMENT

We thank Jules Halpern, Szabi Marka, Imre Bartos, Joe Lazio, Michele Vallisneri and Matthew Graham for useful discussions and suggestions. MC acknowledges support from the National Science Foundation (NSF) NANOGrav Physics Frontier Center, award number 1430284. Financial support was provided by NASA through grants NNX15AB19G, NNX17AL82G, and 16-SWIFT16-0015, and by NSF grant 1715661. Financial support to DJD was provided from NASA through Einstein Postdoctoral Fellowship award number PF6-170151. ZH also gratefully acknowledges support from a Simons Fellowship in Theoretical Physics and hospitality by NYU.

REFERENCES

- Amaro-Seoane P. et al., 2017, ArXiv e-prints
 Artymowicz P., Lubow S. H., 1996, ApJ, 467, L77+
 Barnes J. E., 2002, MNRAS, 333, 481
 Barnes J. E., Hernquist L., 1992, ARA&A, 30, 705
 Begelman M. C., Blandford R. D., Rees M. J., 1980, Nature, 287, 307
 Bianchi S., Chiaberge M., Piconcelli E., Guainazzi M., Matt G., 2008, MNRAS, 386, 105

- Bowen D. B., Campanelli M., Krolik J. H., Mewes V., Noble S. C., 2017a, *ApJ*, 838, 42
- Bowen D. B., Mewes V., Campanelli M., Noble S. C., Krolik J. H., Zilhao M., 2017b, *ArXiv e-prints*
- Caplar N., Lilly S. J., Trakhtenbrot B., 2017, *ApJ*, 834, 111
- Charisi M., Bartos I., Haiman Z., Price-Whelan A. M., Graham M. J., Bellm E. C., Laher R. R., Márka S., 2016, *MNRAS*, 463, 2145
- Charisi M., Bartos I., Haiman Z., Price-Whelan A. M., Márka S., 2015, *MNRAS*, 454, L21
- Colpi M., 2014, *Space Sci. Rev.*, 183, 189
- Comerford J. M., Pooley D., Gerke B. F., Madejski G. M., 2011, *ApJ*, 737, L19
- Cutri R. M., Wisniewski W. Z., Rieke G. H., Lebofsky M. J., 1985, *ApJ*, 296, 423
- D’Orazio D. J., Haiman Z., 2017, *ArXiv e-prints*
- D’Orazio D. J., Haiman Z., Duffell P., Farris B. D., MacFadyen A. I., 2015a, *MNRAS*, 452, 2540
- D’Orazio D. J., Haiman Z., Duffell P., MacFadyen A. I., Farris B. D., 2015b, *ArXiv e-prints*
- D’Orazio D. J., Haiman Z., MacFadyen A., 2013, *MNRAS*, 436, 2997
- D’Orazio D. J., Haiman Z., Schiminovich D., 2015, *Nature*, 525, 351
- D’Orazio D. J., Loeb A., 2017, *ArXiv e-prints*
- Dotti M., Sesana A., Decarli R., 2012, *Advances in Astronomy*, 2012, 940568
- Edelson R., 1992, *ApJ*, 401, 516
- Edelson R. A. et al., 1996, *ApJ*, 470, 364
- Evans I. N., Koratkar A. P., 2004, *ApJS*, 150, 73
- Fabbiano G., Wang J., Elvis M., Risaliti G., 2011, *Nature*, 477, 431
- Farris B. D., Duffell P., MacFadyen A. I., Haiman Z., 2014, *ApJ*, 783, 134
- Fu H., Myers A. D., Djorgovski S. G., Yan L., Wrobel J. M., Stockton A., 2015, *ApJ*, 799, 72
- Giveon U., Maoz D., Kaspi S., Netzer H., Smith P. S., 1999, *MNRAS*, 306, 637
- Gold R., Paschalidis V., Etienne Z. B., Shapiro S. L., Pfeiffer H. P., 2014, *Phys. Rev. D*, 89, 064060
- Goulding A. D. et al., 2017, *ArXiv e-prints*
- Graham M. J., Djorgovski S. G., Drake A. J., Mahabal A. A., Chang M., Stern D., Donalek C., Glikman E., 2014, *MNRAS*, 439, 703
- Graham M. J. et al., 2015a, *MNRAS*, 453, 1562
- Graham M. J. et al., 2015b, *Nature*, 518, 74
- Green P. J., Myers A. D., Barkhouse W. A., Mulchaey J. S., Bennert V. N., Cox T. J., Aldcroft T. L., 2010, *ApJ*, 710, 1578
- Haehnelt M. G., Kauffmann G., 2002, *MNRAS*, 336, L61
- Haiman Z., Kocsis B., Menou K., 2009, *ApJ*, 700, 1952
- Hayasaki K., Mineshige S., Sudou H., 2007, *PASJ*, 59, 427
- Hung T. et al., 2016, *ApJ*, 833, 226
- Ivashchenko G., Sergijenko O., Torbaniuk O., 2014, *MNRAS*, 437, 3343
- Jun H. D., Stern D., Graham M. J., Djorgovski S. G., Mainzer A., Cutri R. M., Drake A. J., Mahabal A. A., 2015, *ApJ*, 814, L12
- Kauffmann G., Haehnelt M., 2000, *MNRAS*, 311, 576
- Kelley L. Z., Blecha L., Hernquist L., 2017, *MNRAS*, 464, 3131
- Kelly B. C., Bechtold J., Siemiginowska A., 2009, *ApJ*, 698, 895
- Kinney A. L., Bohlin R. C., Blades J. C., York D. G., 1991, *ApJS*, 75, 645
- Kocsis B., Haiman Z., Loeb A., 2012a, *MNRAS*, 427, 2680
- Kocsis B., Haiman Z., Loeb A., 2012b, *MNRAS*, 427, 2660
- Komossa S., Burwitz V., Hasinger G., Predehl P., Kaastra J. S., Ikebe Y., 2003, *ApJ*, 582, L15
- Komossa S., Zensus J. A., 2016, in *IAU Symposium*, Vol. 312, *Star Clusters and Black Holes in Galaxies across Cosmic Time*, Meiron Y., Li S., Liu F.-K., Spurzem R., eds., pp. 13–25
- Kormendy J., Ho L. C., 2013, *ARA&A*, 51, 511
- Koss M. et al., 2011, *ApJ*, 735, L42
- Kozłowski S. et al., 2010, *ApJ*, 708, 927
- Kun E., Frey S., Gabányi K. É., Britzen S., Cseh D., Gergely L. Á., 2015, *MNRAS*, 454, 1290
- Kun E., Gabányi K. É., Karouzos M., Britzen S., Gergely L. Á., 2014, *MNRAS*, 445, 1370
- Liu T. et al., 2016, *ApJ*, 833, 6
- Liu T. et al., 2015, *ApJ*, 803, L16
- Lu K.-X., Li Y.-R., Bi S.-L., Wang J.-M., 2016, *MNRAS*, 459, L124
- MacFadyen A. I., Milosavljević M., 2008, *ApJ*, 672, 83
- MacLeod C. L. et al., 2010, *ApJ*, 721, 1014
- Madau P., Ferguson H. C., Dickinson M. E., Gialvalisco M., Steidel C. C., Fruchter A., 1996, *MNRAS*, 283, 1388
- Manchester R. N., IPTA, 2013, *Classical and Quantum Gravity*, 30, 224010
- Mohan P., An T., Frey S., Mangalam A., Gabányi K. É., Kun E., 2016, *MNRAS*, 463, 1812
- Mushotzky R. F., Edelson R., Baumgartner W., Gandhi P., 2011, *ApJ*, 743, L12
- Noble S. C., Mundim B. C., Nakano H., Krolik J. H., Campanelli M., Zlochower Y., Yunes N., 2012, *ApJ*, 755, 51
- Paltani S., Courvoisier T. J.-L., 1994, *A&A*, 291, 74
- Peeples M. S. et al., 2016, in *American Astronomical Society Meeting Abstracts*, Vol. 227, *American Astronomical Society Meeting Abstracts*, p. 444.01
- Rafikov R. R., 2013, *ApJ*, 774, 144
- Rafikov R. R., 2016, *ArXiv e-prints*
- Rodriguez C., Taylor G. B., Zavala R. T., Peck A. B., Pollack L. K., Romani R. W., 2006, *ApJ*, 646, 49
- Roedig C., Sesana A., Dotti M., Cuadra J., Amaro-Seoane P., Haardt F., 2012, *A&A*, 545, A127
- Ruan J. J., Anderson S. F., Dexter J., Agol E., 2014, *ApJ*, 783, 105
- Ryan G., MacFadyen A., 2017, *ApJ*, 835, 199
- Sakata Y., Morokuma T., Minezaki T., Yoshii Y., Kobayashi Y., Koshida S., Sameshima H., 2011, *ApJ*, 731, 50
- Sesana A., Haiman Z., Kocsis B., Kelley L. Z., 2017, *ArXiv e-prints*
- Shull J. M., Stevans M., Danforth C. W., 2012, *ApJ*, 752, 162
- Simm T., Salvato M., Saglia R., Ponti G., Lanzuisi G., Trakhtenbrot B., Nandra K., Bender R., 2016, *A&A*, 585, A129
- Tang Y., Haiman Z., MacFadyen A., 2018, *ArXiv e-prints*
- Tang Y., MacFadyen A., Haiman Z., 2017, *MNRAS*, 469, 4258
- Vanden Berk D. E. et al., 2004, *ApJ*, 601, 692
- Vaughan S., Uttley P., Markowitz A. G., Huppenkothen D., Middleton M. J., Alston W. N., Scargle J. D., Farr W. M., 2016, *MNRAS*, 461, 3145
- Welsh B. Y., Wheatley J. M., Neil J. D., 2011, *A&A*, 527, A15
- Wilhite B. C., Vanden Berk D. E., Kron R. G., Schneider D. P., Pereyra N., Brunner R. J., Richards G. T., Brinkmann J. V., 2005, *ApJ*, 633, 638
- Wilson E. B., 1927, *Journal of the American Statistical Association*, 22, 209
- Zheng Z.-Y., Butler N. R., Shen Y., Jiang L., Wang J.-X., Chen X., Cuadra J., 2016, *ApJ*, 827, 56
- Zhu F.-F., Wang J.-X., Cai Z.-Y., Sun Y.-H., 2016, *ApJ*, 832, 75
- Zu Y., Kochanek C. S., Kozłowski S., Udalski A., 2013, *ApJ*, 765, 106

Table 2. Properties of periodic quasars analysed for relativistic Doppler boost.

#	Name	A_{opt}	α_{opt}	$A_{\text{nUV}}/A_{\text{opt}}$	α_{nUV}	$A_{\text{fUV}}/A_{\text{opt}}$	α_{fUV}	$\frac{A_{\text{Dop}} _{\text{max}}}{2A_{\text{opt}}}$
1	SDSS J110554.78+322953.7	0.11±0.009	-1.56±0.09	5.91±0.71	-23.94±3.24	7.80±1.82	-32.56±8.29	1.62
2	SDSS J131706.19+271416.7	0.12±0.011	-0.27±0.12	7.61±4.96	-21.92±16.25	—	—	5.45
3	SDSS J072908.71+400836.6	0.06±0.005	-3.67±0.01	3.70±2.48	-21.72±16.52	—	—	0.65
4	3C 298.0	0.08±0.005	-1.15±0.01	5.18±0.72	-18.49±2.98	3.97±2.04	-13.47±8.48	6.44
5	SDSS J114438.34+262609.4	0.16±0.013	-1.16±0.01	4.12±1.05	-14.14±4.38	-0.29±5.10	4.19±21.20	3.18
6	SDSS J081133.43+065558.1	0.18±0.014	-1.37±0.01	3.26±0.28	-11.26±1.22	—	—	2.81
7	SDSS J153636.22+044127.0	0.09±0.008	-1.01±0.01	3.31±0.75	-10.30±3.02	—	—	3.20
8	BZQ J0842+4525	0.10±0.005	-1.46±0.01	2.46±0.89	-7.98±3.96	1.82±2.30	-5.12±10.27	5.34
9	SDSS J140704.43+273556.6	0.11±0.007	-0.58±0.01	2.92±0.70	-7.46±2.51	—	—	6.59
10	SDSS J130040.62+172758.4	0.30±0.022	-0.65±0.01	2.63±0.68	-6.61±2.50	—	—	0.86
11	SDSS J131909.08+090814.7	0.13±0.011	-0.90±0.01	2.41±1.09	-6.41±4.23	—	—	2.10
12	SDSS J125414.23+131348.1	0.16±0.012	-0.08±0.06	3.04±0.40	-6.37±1.24	—	—	1.42
13	SDSS J142301.96+101500.1	0.14±0.010	-1.29±0.05	2.18±0.73	-6.35±3.15	—	—	4.08
14	QNZ 3:54	0.19±0.013	-0.74±0.18	2.48±0.15	-6.26±0.57	1.49±0.41	-2.57±1.52	2.25
15	SDSS J104941.01+085548.4	0.16±0.009	-0.64±0.01	2.42±0.39	-5.81±1.43	—	—	2.86
16	SDSS J082121.88+250817.5	0.09±0.007	0.17±0.01	2.98±1.26	-5.45±3.66	2.87±2.56	-5.14±7.24	4.21
17	SDSS J081617.73+293639.6	0.14±0.012	-0.85±0.01	2.15±0.54	-5.29±2.10	—	—	4.51
18	SDSS J133654.44+171040.3	0.13±0.010	-1.14±0.01	1.94±0.41	-5.04±1.71	—	—	3.50
19	SDSS J102255.21+172155.7	0.13±0.014	-0.99±0.12	1.96±0.37	-4.81±1.49	—	—	1.79
20	SDSS J083349.55+232809.0	0.09±0.008	-1.21±0.01	1.71±0.47	-4.21±1.96	2.79±1.16	-8.74±4.88	6.11
21	SDSS J104430.25+051857.2	0.09±0.007	-1.05±0.01	1.72±0.94	-3.96±3.81	0.34±2.56	1.64±10.35	5.06
22*	SDSS J170942.58+342316.2	0.18±0.014	-1.56±0.01	1.48±1.13	-3.77±5.17	—	—	4.93
23	HS 0926+3608	0.08±0.006	-0.39±0.08	1.98±1.20	-3.73±4.07	—	—	9.11
24	RXJ J10304+5516	0.08±0.008	-0.48±0.01	1.92±0.66	-3.67±2.28	3.26±0.80	-8.34±2.78	2.33
25	SDSS J121018.34+015405.9	0.12±0.009	-0.22±0.01	1.91±0.24	-3.14±0.76	1.21±0.24	-0.88±0.79	1.45
26	SDSS J092911.35+203708.5	0.21±0.014	-0.22±0.01	1.87±1.81	-3.03±5.84	-0.65±2.95	5.11±9.51	2.76
27	SDSS J224829.47+144418.0	0.32±0.019	0.39±0.01	2.25±0.26	-2.88±0.68	—	—	0.61
28	SDSS J104758.34+284555.8**	0.30±0.018	-0.32±0.01	1.73±0.73	-2.76±2.43	—	—	0.65
29	SDSS J144754.62+132610.0**	0.17±0.015	0.25±0.01	1.99±0.32	-2.47±0.87	—	—	0.85
30	SDSS J161013.67+311756.4	0.09±0.006	-0.99±0.01	1.36±0.96	-2.45±3.82	6.99±2.74	-24.93±10.94	1.38
31	SDSS J094450.76+151236.9	0.11±0.008	-0.18±0.08	1.62±0.57	-2.16±1.83	—	—	4.24
32	SDSS J121457.39+132024.3	0.20±0.012	-0.50±0.01	1.47±0.15	-2.14±0.53	—	—	2.09
33	SDSS J082926.01+180020.7**	0.22±0.015	-0.20±0.01	1.57±0.57	-2.02±1.89	—	—	0.84
34	SDSS J154409.61+024040.0	0.27±0.018	-1.25±0.01	1.12±0.25	-1.77±1.06	—	—	1.13
35	SDSS J140600.26+013252.2**	0.16±0.014	0.07±0.01	1.56±0.19	-1.58±0.54	1.07±0.30	-0.12±0.89	0.81
36	SDSS J170616.24+370927.0	0.13±0.012	-1.15±0.01	1.08±0.22	-1.47±0.91	—	—	2.99
37	SDSS J121018.66+185726.0	0.08±0.008	-0.95±0.01	0.97±1.15	-0.82±4.56	-2.47±2.85	12.77±11.25	6.52
38	HS 1630+2355	0.08±0.004	-0.78±0.01	0.95±0.44	-0.60±1.68	—	—	6.34
39	SDSS J160730.33+144904.3	0.12±0.010	0.06±0.01	1.20±1.02	-0.52±3.00	-0.01±3.48	3.04±10.21	4.24
40	SDSS J221016.97+122213.9	0.22±0.017	0.33±0.01	1.25±0.25	-0.34±0.68	7.85±1.93	-17.95±5.15	1.05
41	SDSS J150450.16+012215.5	0.14±0.009	-1.78±0.01	0.67±0.19	-0.22±0.93	0.57±0.41	0.28±1.98	3.58
42*	SDSS J171617.49+341553.3	0.14±0.012	-0.38±0.02	0.95±0.99	-0.20±3.34	—	—	6.07
43	US 3204	0.20±0.013	-0.80±0.01	0.84±0.29	-0.18±1.11	1.60±0.66	-3.10±2.50	1.61
44	SDSS J133631.45+175613.8	0.14±0.011	-0.14±0.02	0.94±1.69	0.06±5.29	—	—	1.66
45	SDSS J135225.80+132853.2	0.11±0.007	-0.13±0.02	0.93±1.20	0.09±3.77	—	—	1.61
46	UM 234	0.17±0.011	-0.34±0.01	0.83±0.19	0.23±0.63	2.08±0.30	-3.96±1.01	1.70
47*	SDSS J231733.66+001128.3	0.23±0.006	-0.38±0.01	0.79±0.15	0.32±0.54	1.82±0.97	-3.17±3.32	1.64
48	SDSS J124157.90+130104.1	0.21±0.015	-1.38±0.02	0.61±0.28	0.35±1.23	—	—	1.77
49	SDSS J082716.85+490534.0**	0.24±0.019	0.05±0.01	0.69±0.21	0.96±0.62	1.31±0.94	-0.87±2.77	0.94
50*	SDSS J005158.83-002054.1	0.21±0.009	0.08±0.01	0.65±0.43	1.09±1.26	—	—	1.53
51*	SDSS J212939.60+004845.5	0.21±0.014	0.04±0.01	0.63±0.16	1.13±0.46	0.46±3.26	1.64±9.67	2.93
52	SDSS J103111.52+491926.5	0.08±0.008	-1.21±0.01	0.36±0.59	1.51±2.48	—	—	4.83
53	SDSS J143820.60+055447.9	0.23±0.016	-0.01±0.01	0.35±0.30	1.95±0.91	0.36±0.51	1.91±1.53	0.50
54*	PDS 898	0.27±0.011	0.42±0.01	0.38±0.12	2.01±0.30	—	—	1.01
55	PGC 3096192	0.08±0.009	-0.39±0.01	0.09±0.39	2.70±1.32	5.86±2.83	-16.88±9.58	0.75
56	SDSS J084146.19+503601.1	0.19±0.013	0.61±0.01	0.09±0.24	2.79±0.58	—	—	0.28
57	SDSS J164452.71+430752.2	0.13±0.011	-1.20±0.07	-0.02±0.70	3.07±2.92	—	—	7.34
58*	UM 269	0.34±0.006	-0.52±0.01	-0.02±0.29	3.09±1.02	-0.23±0.39	3.80±1.36	0.69
59	SDSS J152157.02+181018.6	0.12±0.011	-0.64±0.01	-0.33±0.66	4.21±2.40	—	—	0.98
60	HS 0946+4845	0.12±0.007	0.01±0.01	-0.54±0.32	4.63±0.95	—	—	1.39
61*	SDSS J235958.72+003345.3	0.22±0.012	-1.43±0.01	-0.38±0.29	4.66±1.28	—	—	2.87
62*	SDSS J024442.77-004223.2	0.29±0.018	-0.81±0.04	-0.45±0.14	4.72±0.52	4.31±2.51	-13.42±9.55	0.87
63*	SDSS J141004.41+334945.5	0.21±0.006	0.26±0.01	-0.71±0.24	4.94±0.67	—	—	1.40
64*	SDSS J235928.99+170426.9	0.35±0.019	0.51±0.01	-1.07±0.40	5.66±0.99	0.93±1.26	0.69±3.13	0.99
65	SDSS J133516.17+183341.4	0.12±0.011	-0.86±0.01	-0.84±0.93	6.22±3.58	—	—	4.83
66*	SDSS J214036.77+005210.1	0.17±0.012	-0.34±0.24	-0.97±0.64	6.25±2.13	—	—	2.62
67	SDSS J123147.27+101705.3	0.24±0.016	-0.31±0.01	-2.18±1.21	10.23±4.00	—	—	1.38
68*	SDSS J171122.67+342658.9	0.33±0.020	0.06±0.01	-3.08±1.15	12.03±3.38	—	—	1.44

We emphasize with bold the sources that are consistent with relativistic Doppler boost.

* SMBHB candidates identified in PTF (C16).

** Sources that were consistent with the multi-wavelength prediction of Doppler boost, but not with the maximum amplitude requirement.